mathematics

MDPI

Article

Slip Effects on MHD Squeezing Flow of Jeffrey Nanofluid in Horizontal Channel with Chemical Reaction

Nur Azlina Mat Noor, Sharidan Shafie and Mohd Ariff Admon *

Department of Mathematical Sciences, Faculty of Science, Universiti Teknologi Malaysia, Johor Bahru 81310, Johor, Malaysia; nurazlinamatnoor@yahoo.com (N.A.M.N.); sharidan@utm.my (S.S.)
* Correspondence: ariffadmon@utm.my

Abstract: The heat and mass transfer characteristics on hydromagnetic squeeze flow of Jeffrey nanofluid between two plates over a permeable medium by slip condition with the influences of viscous dissipation and chemical reaction is examined. Buongiorno's nanofluid model, which includes Brownian motion and thermophoresis impacts, is implemented in this research. The governing nonlinear partial differential equations are transformed to the nonlinear ordinary differential equations via asimilarity transformation. The transformed equations are solved by employing numerical techniques of Keller-box. A comparison of the skin friction coefficient, Nusselt and Sherwood numbers with reported outputs in the journals are carried out to validate the present outputs. An excellent agreement is found. The results show that the squeezing of plates accelerates the velocity and wall shear stress. Furthermore, the velocity, temperature and concentration profile decrease when the Hartmann number and ratio of relaxation and retardation times increases. The raise in thermophoresis and viscous dissipation elevate the temperature profile and the heat transfer rate. Furthermore, the mass transfer rate declines due to the strong Brownian motion in the nanofluid, whereas it increases with the addition of chemical reaction and thermophoresis.

Keywords: squeezing flow; Jeffrey nanofluid; slip condition; viscous dissipation; chemical reaction

Citation: Mat Noor, N.A.; Shafie, S.; Admon, M.A. Slip Effects on MHD Squeezing Flow of Jeffrey Nanofluid in Horizontal Channel with Chemical Reaction. *Mathematics* **2021**, *9*, 1215. https://doi.org/10.3390/math9111215

Academic Editors: Mahdi Bodaghi and Ricardo Lopez-Ruiz

Received: 22 February 2021
Accepted: 23 April 2021
Published: 27 May 2021

1. Introduction

The development of an innovative heat transfer fluid is significant for achieving the cooling rate standards in the current industries. Nanofluid is an engineered colloid consisting of solid nanoparticles (1–100 nm) suspended in a conventional fluid, for instance, ethylene glycol, water or engine oil. The conventional fluid has limited heat transfer capability owing to the low thermal conductivity. Therefore, the dispersion of metallic nanoparticles in the fluid is implemented to boost the thermal conductivity of the conventional fluid. Eastman et al. [1] stated that the addition of copper nanoparticles increases the thermal conductivity of ethylene glycol up to 40% because the suspended nanoparticles enhance the ability of energy exchange in the flow. Nanofluid has been used in many industrial applications, such as nanodrug delivery, lowering fuel in electric power plants and vehicle cooling. Wong and De Leon [2] reported that nanofluid coolants contribute to better energy savings and emission reductions. The analysis on seven slip mechanisms, which generate a relative velocity amongst nanoparticles and base fluid, was carried out by Buongiorno [3]. It was discovered that only Brownian motion and thermophoresis are substantial for improving the heat transfer process in nanofluid. Later, Buongiorno's model was employed by many scientists to explore the convective flow of nanofluid [4–6].

Squeezing flow is caused by the motion of two parallel plates or boundaries with normal external stress. The idea of squeeze flow has been investigated extensively due to its engineering and industrial applications, for example, moving pistons, lubrication systems, hydraulic lifts and injection molding. Stefan [7] began the study on the behavior of lubricant within two squeezing plates using lubrication theory. Based on the pioneer works of Stefan, the study on squeezing flow is explored for various geometries. Reynolds [8] and

Archibald [9] continued Stefan's work by considering elliptical and rectangular geometries, respectively. Reynolds equation was used as the governing equations of the mathematical model in the previous studies. However, Jackson [10] and Ishizawa [11] reviewed that the Reynolds equation is inappropriate when applied in the squeezing flow with high velocity and porous thrust bearings. Hence, several renewed studies were done to revise the fundamental model of squeezing flow mathematically [12–17].

Jeffrey fluid is categorized as non-Newtonian fluid based on the flow behavior, which correlated with the relationship of shear stress and strain. It is shear thinning flow with yield stress and high shear viscosity. The fluid acts as a solid if the applied stress exerted is lower than the yield stress, whereas the fluid begins to flow if the applied stress exerted is more than yield stress [18]. Jeffrey fluid is a simple linear model where time derivatives are used as a substitute for convective derivatives. The viscoelastic properties in the polymer industry are described by the relaxation and retardation times parameter [19]. Furthermore, the blood flow in narrow arteries is treated as Jeffrey fluid because of the rheological characteristics [20].

The studies of MHD boundary layer flow has received great interest in engineering application involving MHD pump and generator. The induction of Lorentz force occurs when a magnetic field is imposed on the electrically conducting fluid. The Lorentz forces are useful in regulating momentum and heat transfer flow in the boundary region [21]. The influence of suction and injection on an unsteady MHD squeeze flow of Jeffrey fluid across a permeable channel was analyzed by Hayat et al. [22]. The series solution is obtained via the homotopy analysis method (HAM). Then, Muhammad et al. [23] extended Hayat et al. [22] research with magnetic field on squeezing flow of Jeffrey fluid with stretching lower plate. The numerical solution of mixed convection of Jeffrey fluid at a stagnation point was presented by Ahmad and Ishak [24] using Keller-box technique. The flow is produced by a stretched vertical plate with a transverse magnetic field. Further, Hayat et al. [25] investigated the squeezing flow of Jeffrey nanofluid through two disks with a magnetic field effect.

Viscous dissipation is known as the irreversible process of mechanical energy converted to thermal energy due to internal friction in the viscous flow. It is only significant for the fluid with high velocity and viscosity. The presence of viscous dissipation on an unsteady squeeze flow of nanofluid within two plates was examined by Sheikholeslami et al. [26], Pourmehran et al. [27] and Gorgani et al. [28]. They used Tiwari and Das model with different types of methods to obtain the solution. Acharya et al. [29] reported the squeezing nanofluid flow with the combined impacts of viscous dissipation and magnetic field via the Tiwari and Das model. Meanwhile, Azimi and Riazi [30] solved the same problem via Buongiorno's model. Later, Sheikholeslami et al. [31] extended Acharya et al. [29] work by considering thermal radiation impact. Madaki et al. [32] explored the influences of viscous dissipation and thermal radiation on the squeezing flow of the nanofluid via the Tiwari and Das model.

All the above-mentioned studies involved with no slip condition at the plate. However, the momentum slip at the wall is important for the fluid that exhibits elastic characteristics. The physical situations that possess slip conditions are the flow in the micro devices, polishing of internal cavities and artificial heart valves [33]. The momentum slip occurs when the velocity of the wall is no longer the same as the fluid velocity adjacent to the wall. Khan et al. [34] discovered the impact of velocity slip on the squeeze flow of the nanofluid in two plates with viscous dissipation. Furthermore, Singh et al. [35] extended Khan et al.'s [34] studies by including a magnetic field. The research on an unsteady MHD nanofluid flow caused by the squeezing of two parallel disks with a velocity slip was discussed by Sobamowo and Jayesimi [36]. Further, Sobamowo et al. [37] continued the study of Sobamowo and Jayesimi [36] by considering squeezing nanofluid flow over permeable medium with suction and injection under the influence of a velocity and temperature slip.

Another significant characteristic that affects the flow behavior is mass transfer involving a chemical reaction. Several examples of chemical reaction applications are solar

collectors, nuclear reactor safety, damage of crop equipment and the design of the chemical process [38]. Many researchers have explored the chemical reaction impacts on nanofluid flow for various geometries. Ullah et al. [39] analyzed the influences of a chemical reaction and thermal radiation on the MHD squeeze flow of a nanofluid in the two disks with suction and injection. The analytical solution of MHD squeeze flow of nanofluid over two plates across permeable medium with chemical reaction, thermal radiation, viscous dissipation and heat source or sink was studied by Mohamed et al. [40]. In non-Newtonian fluid, Raju et al. [41] discussed the presence of a chemical reaction, magnetic field and thermal radiation on a mixed convection flow of a Jeffrey nanofluid across a permeable cone. Further, the squeeze flow of Casson nanofluid within two plates with the effects of MHD, joule heating, viscous dissipation and a chemical reaction was examined by Shankar and Naduvinamani [42]. Later, Noor et al. [43] extended Shankar and Naduvinamani's [42] work by considering the squeeze flow of a Casson nanofluid over a permeable medium with a heat source or sink.

The literature discussion above reveals that most of the previous studies on an unsteady squeeze flow within two plates are done for nanofluid. The study involving Jeffrey nanofluid is limited. Furthermore, the combined impacts of viscous dissipation and chemical reaction on squeeze flow of the Jeffrey nanofluid have not yet been considered. Hence, the present research concentrates on an unsteady squeeze flow of MHD Jeffrey nanofluid through a permeable medium under the effects of viscous dissipation and chemical reaction. The velocity slip boundary condition is considered. Similarity transformations are imposed to convert the partial differential equations into the non-dimensional form and are solved by the Keller-box technique. The results computed from MATLAB are compared with existing outputs from the literature. The velocity, temperature and nanoparticle concentration fields are observed with different related parameters.

The present work is mostly implemented in the modeling of nuclear reactor safety. It is designed to terminate the nuclear reaction automatically when hazards occur. The flow with a chemical reaction is suitable to be used as a model for the nuclear reactor protection system [38]. Furthermore, the electricity generated by a nuclear reactor increases when a magnetic field is imposed on the system [44]. The presence of nanofluid is important in a nuclear power plant to improve the heat transfer process. Heat transfer capacity in a nuclear reactor is a thousand times larger than conventional fluids due to the high thermal conductivity of the nanofluid. It increases the efficiency of the nuclear reactor and reduces the thermal hydraulic problems. A new gateway for the high energy optimization has been discovered with nanofluid [45].

2. Mathematical Formulation

The unsteady MHD flow of Jeffrey nanofluid through a permeable medium with a chemical reaction and viscous dissipation impacts. The velocity slip is located at the upper plate. The compression of two plates generates the fluid flow. The distance of two plates is $y = \pm h(t) = \pm l(1 - \alpha t)^{1/2}$. The upper and lower plates approach closer with velocity $v_w(t) = \dfrac{\partial h(t)}{\partial t}$. The two plates are separated as $\alpha < 0$, and the plates are squeezed as $\alpha > 0$ until $t = 1/\alpha$. The magnetic field $B(t) = B_0(1 - \alpha t)^{-1/2}$ is applied to the electrically conducting fluid through the lower plate. Figure 1 illustrates the coordinate system and geometrical model for the squeeze flow of the Jeffrey nanofluid.

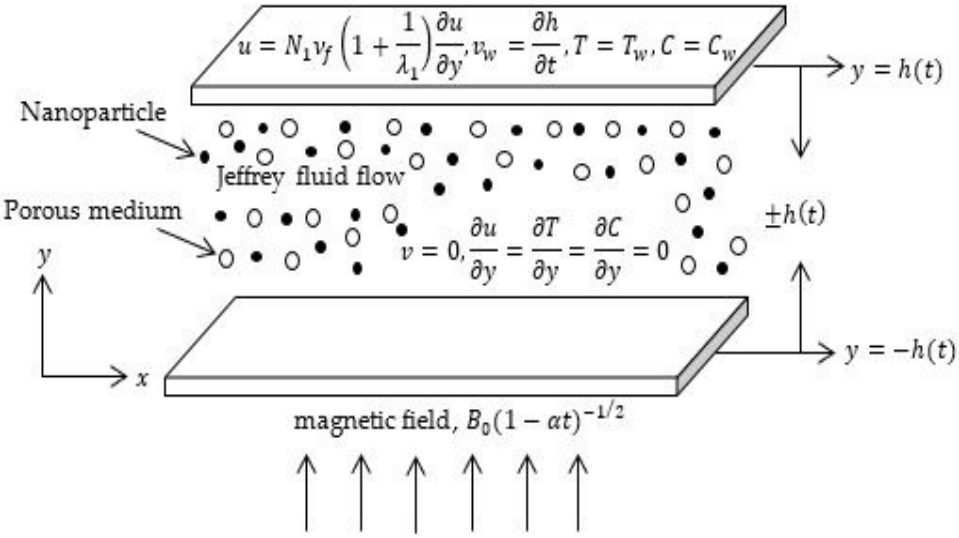

Figure 1. Geometrical model.

Based on the boundary layer approximations, the continuity, momentum, energy and concentration equations of Jeffrey nanofluid are

$$\frac{\partial u}{\partial x} + \frac{\partial v}{\partial y} = 0, \tag{1}$$

$$\begin{aligned}\frac{\partial u}{\partial t} + u\frac{\partial u}{\partial x} + v\frac{\partial u}{\partial y} =& \nu_f\left(1 + \frac{1}{\lambda_1}\right)\frac{\partial^2 u}{\partial y^2} + \nu_f\frac{\lambda_2}{1+\lambda_1}\left(\frac{\partial^3 u}{\partial t \partial y^2} + u\frac{\partial^3 u}{\partial x \partial y^2}\right.\\ &\left. + v\frac{\partial^3 u}{\partial y^3} - \frac{\partial u}{\partial x}\frac{\partial^2 u}{\partial y^2} + \frac{\partial u}{\partial y}\frac{\partial^2 u}{\partial x \partial y}\right) - \frac{\sigma B^2(t)}{\rho_f}u\\ &- \nu_f\left(1 + \frac{1}{\lambda_1}\right)\frac{\varphi}{k_1(t)}u,\end{aligned} \tag{2}$$

$$\begin{aligned}\frac{\partial T}{\partial t} + u\frac{\partial T}{\partial x} + v\frac{\partial T}{\partial y} =& \alpha_f\frac{\partial^2 T}{\partial y^2} + \tau\left[D_B\frac{\partial C}{\partial y}\frac{\partial T}{\partial y} + \frac{D_T}{T_m}\left(\frac{\partial T}{\partial y}\right)^2\right]\\ &+ \frac{\nu_f}{c_f}\left(1 + \frac{1}{\lambda_1}\right)\left[4\left(\frac{\partial u}{\partial x}\right)^2 + \left(\frac{\partial u}{\partial y}\right)^2\right],\end{aligned} \tag{3}$$

$$\frac{\partial C}{\partial t} + u\frac{\partial C}{\partial x} + v\frac{\partial C}{\partial y} = D_B\frac{\partial^2 C}{\partial y^2} + \frac{D_T}{T_m}\frac{\partial^2 T}{\partial y^2} - k_c(t)C, \tag{4}$$

Here, $k_1(t) = k_0(1 - \alpha t)$ is the permeability of porous medium, $\alpha_f = \dfrac{k}{(\rho c)_f}$ is the thermal diffusivity of the Jeffrey fluid, $\tau = \dfrac{(\rho c)_p}{(\rho c)_f}$ is the ratio of the heat capacities of nanoparticles and fluid and $k_c(t) = k_2(1 - \alpha t)^{-1}$ is the chemical reaction rate.

The corresponded boundary conditions are

$$u = N_1 v_f\left(1 + \frac{1}{\lambda_1}\right)\frac{\partial u}{\partial y}, v = v_w = \frac{\partial h(t)}{\partial t}, T = T_w, C = C_w, \quad \text{at} \quad y = h(t), \tag{5}$$

$$\frac{\partial u}{\partial y} = 0, \frac{\partial^3 u}{\partial y^3} = 0, v = 0, \frac{\partial T}{\partial y} = 0, \frac{\partial C}{\partial y} = 0, \qquad \text{at} \qquad y = 0, \tag{6}$$

where $N_1(t) = N_0(1 - \alpha t)^{1/2}$ represents the momentum slip.

The non-dimensional variables are implemented to reduce the partial differential equations into ordinary differential equations [46];

$$\begin{aligned}\eta &= \frac{y}{l\sqrt{(1-\alpha t)}}, u = \frac{\alpha x}{2(1-\alpha t)}f'(\eta), v = \frac{\alpha l}{2\sqrt{(1-\alpha t)}}f(\eta),\\ \theta &= \frac{T}{T_w}, \phi = \frac{C}{C_w},\end{aligned} \tag{7}$$

Substituting the dimensionless variables of Equation (7) into Equations (2)–(4) yields

$$\begin{aligned}&\left(1+\frac{1}{\lambda_1}\right)f^{iv} - S(\eta f''' + 3f'' + f'f'' - ff''')\\ &+ \left(1+\frac{1}{\lambda_1}\right)\frac{De}{2}(\eta f^v + 5f^{iv} + 2f''f''' - f'f^{iv} - ff^v) - Ha^2 f''\\ &- \left(1+\frac{1}{\lambda_1}\right)\frac{1}{Da}f'' = 0,\end{aligned} \tag{8}$$

$$\begin{aligned}&\frac{1}{Pr}\left(1+\frac{4}{3}R_d\right)\theta'' + S(f\theta' - \eta\theta') + Ec\left[\left(1+\frac{1}{\lambda_1}\right)[(f'')^2 + 4\delta^2(f')^2]\right]\\ &+ N_b\phi'\theta' + N_t(\theta')^2 = 0,\end{aligned} \tag{9}$$

$$\frac{1}{Le}\phi'' + S(f\phi' - \eta\phi') + \frac{1}{Le}\frac{N_t}{N_b}\theta'' - R\phi = 0, \tag{10}$$

with the non-dimensional boundary conditions

$$f(\eta) = 0, f''(\eta) = 0, f^{iv}(\eta) = 0, \theta'(\eta) = 0, \phi'(\eta) = 0, \quad \text{at} \quad \eta = 0, \tag{11}$$

$$f(\eta) = 1, f'(\eta) = \gamma\left(1+\frac{1}{\lambda_1}\right)f''(\eta), \theta(\eta) = 1, \phi(\eta) = 1, \quad \text{at} \quad \eta = 1. \tag{12}$$

The significant parameters in the non-dimensional equations are defined as

$$\begin{aligned}&S = \frac{\alpha l^2}{2\nu_f}, Ha = lB_0\sqrt{\frac{\sigma}{\rho_f\nu_f}}, Da = \frac{k_0}{\varphi l^2}, De = \frac{\alpha\lambda_2}{1-\alpha t},\\ &\delta = \frac{l}{x}(1-\alpha t)^{1/2}, Pr = \frac{v_f}{\alpha_f}, Ec = \frac{\alpha^2 x^2}{4c_f T_w(1-\alpha t)^2},\\ &Le = \frac{\nu_f}{D_B}, N_b = \frac{\tau D_B C_w}{\nu_f}, N_t = \frac{\tau D_t T_w}{\nu_f T_m},\\ &R = \frac{k_2 l^2}{\nu_f}, \gamma = \frac{N_0\nu_f}{l}.\end{aligned} \tag{13}$$

Physically, the movement of the channel is portrayed by a squeezing number, where $S > 0$ shows the plates moving nearer and $S < 0$ shows the plates moving further. Deborah, Hartmann and Darcy numbers are used to manage the fluid velocity. Moreover, Prandtl and Eckert numbers are significant in regulating fluid temperature. The nanoparticle concentration is discovered by a chemical reaction parameter. Furthermore, the flow at the simultaneous momentum and mass diffusion is described by the Lewis number.

3. Results and Discussion

The ordinary differential Equations (8)–(10) with corresponding boundary conditions (11) and (12) are solved using the Keller-box scheme. The numerical and graphical results are attained via MATLAB software. A proper guess of the step size $\Delta\eta = 0.01$ and boundary layer thickness $\eta_\infty = 1$ is considered to achieve precise results. The difference between the previous and

present outputs of velocity, temperature and concentration is known as convergence criteria. The iteration is stopped for all the values when it converged to [43].

The computations are discovered for S, λ_1, Ha, Da, γ, De, Pr, Ec, N_b, N_t, Le and R to examine the physical behavior of the velocity, temperature and nanoparticle concentration. Tables 1–3 portray that the present results are compared with the reported outputs of the journals as limiting cases.

The numerical results of the skin friction coefficient for S are compared with Wang [14] and Khan et al. [17] in Table 1. The comparison of skin friction coefficient, Nusselt and Sherwood numbers for S are presented in Table 2 with Naduvinamani and Shankar [47]. Table 3 depicts that the Nusselt number is compared with Mustafa et al. [48], Gupta and Ray [49] and Celik [50] for Pr and Ec values. Good agreement is noticed from the numerical results shown in Tables 1–3.

Table 1. Numerical outputs of $-f''(1)$ for S as $\lambda_1 \to \infty$, $Da \to \infty$, $De = N_b = 10^{-10}$, $Ha = \gamma = Ec = \delta = N_t = R = 0$ and $Pr = Le = 1$.

	$-f''(1)$		
S	**Wang [14]**	**Khan et al. [17]**	**Present Results**
−0.9780	2.235	2.1915	2.1917
−0.4977	2.6272	2.6193	2.6194
−0.09998	2.9279	2.9277	2.9277
0	3.000	3.000	3.000
0.09403	3.0665	3.0663	3.0664
0.4341	3.2969	3.2943	3.2943
1.1224	3.714	3.708	3.708

Table 2. Numerical outputs of $-f''(1)$, $-\theta'(1)$ and $-\phi'(1)$ for S as $\lambda_1 \to \infty$, $Da \to \infty$, $De = N_b = 10^{-10}$, $Ha = \gamma = N_t = 0$, $\delta = 0.1$ and $Pr = Ec = Le = R = 1$.

	Naduvinamani and Shankar [47]			**Present Outputs**		
S	$-f''(1)$	$-\theta'(1)$	$-\phi'(1)$	$-f''(1)$	$-\theta'(1)$	$-\phi'(1)$
−1.0	2.170091	3.319899	0.804559	2.170255	3.319904	0.804558
−0.5	2.617404	3.129491	0.781402	2.617512	3.129556	0.781404
0.01	3.007134	3.047092	0.761225	3.007208	3.047166	0.761229
0.5	3.336449	3.026324	0.744224	3.336504	3.026389	0.744229
2.0	4.167389	3.118551	0.701813	4.167412	3.118564	0.701819

Table 3. Numerical outputs of the Nusselt number for Pr and Ec when $\lambda_1 \to \infty$, $Da \to \infty$, $De = N_b = 10^{-10}$, $Ha = \gamma = N_t = 0$, $\delta = 0.1$, $S = 0.5$ and $Le = R = 1$.

		$-\theta'(1)$			
Pr	Ec	**Mustafa et al. [48]**	**Gupta and Ray [49]**	**Celik [50]**	**Present Results**
0.5	1.0	1.522368	1.522367	1.522367	1.522401
1.0	1.0	3.026324	3.026323	3.026324	3.026389
2.0	1.0	5.980530	5.980530	5.980530	5.980652
5.0	1.0	14.43941	14.43941	14.43941	14.43965
1.0	0.5	1.513162	1.513162	1.513162	1.513194
1.0	1.2	3.631588	3.631588	3.631588	3.631667
1.0	2.0	6.052647	6.052647	6.052647	6.052778
1.0	5.0	15.13162	15.13162	15.13162	15.13194

Figures 2–5 present the variation of S on velocity, temperature, and concentration. The movement of plates closer to each other is represented by $S > 0$, and the separation of plates from each other is represented by $S < 0$. The normal velocity displayed in Figure 2

decreases as $S > 0$, whereas the velocity increases as $S < 0$ in the vicinity $0 \leq \eta \leq 1$. It is discovered that the fluid is squeezed into the channel as the surfaces move further, which results in enhancing the flow velocity. In contrast, the reduction of velocity caused by the fluid is squeezed out from the channel as the plates move nearer. The impact of S on axial velocity is exhibited in Figure 3. The vicinity adjacent to the lower wall is $0 \leq \eta < 0.45$, and the vicinity adjacent to the upper wall is $0.45 \leq \eta \leq 1$. The velocity is shown decelerating for $\eta < 0.45$, and it accelerates for $\eta \leq 0.45$ when $S > 0$. In contrast, the velocity elevating for $\eta < 0.45$ and it declines for $\eta \geq 0.45$ when $S < 0$. It is discovered that the squeeze of plates leads to the flow over the narrow channel at a fast rate. Meanwhile, the fluid velocity slows down due to the flow encounters high opposition in the wider channel. It is explored that the crossflow arises at the center of the channel. It is found that for the velocity profile at $\eta_c = 0.45$, the critical point is not affected when varying the squeeze parameter. The variation of S on the temperature field is portrayed in Figure 4. The temperature profile drops when the plates move closer $(S > 0)$ because the smaller volume of the channel reduces the kinetic energy of fluid particles. Furthermore, the movement of plates further from one another $(S < 0)$ promotes the kinetic energy and, therefore, elevates the temperature in the flow. The kinetic energy is directly proportional to temperature. It is noticed that the fluid temperature is constant adjacent to the upper wall. Figure 5 depicts the influence of S on nanoparticle concentration. The concentration profile rises when $S > 0$ and it declines when $S < 0$.

The influences of λ_1 on velocity, temperature, and concentration are exhibited in Figures 6–9. The radial velocity in Figure 6 decelerating with a rise in λ_1. The reason is that an increase in λ_1 enhances the intermolecular forces within fluid particles, which increases the viscosity of the fluid. The axial velocity presented in Figure 7 decreases for $\eta \leq 0.5$ and it increases for $\eta > 0.5$ when λ_1 rises. The cross behavior of flow occurs at the middle of the boundary layer. Figure 8 depicts the effect of λ_1 on the temperature field. The flow temperature declines as λ_1 rises. The increase in fluid viscosity implies stronger intermolecular forces and, consequently, reduces the kinetic energy of fluid particles. Figure 9 demonstrates the influence of λ_1 on the concentration field. The increment of λ_1 elevates the nanoparticle concentration.

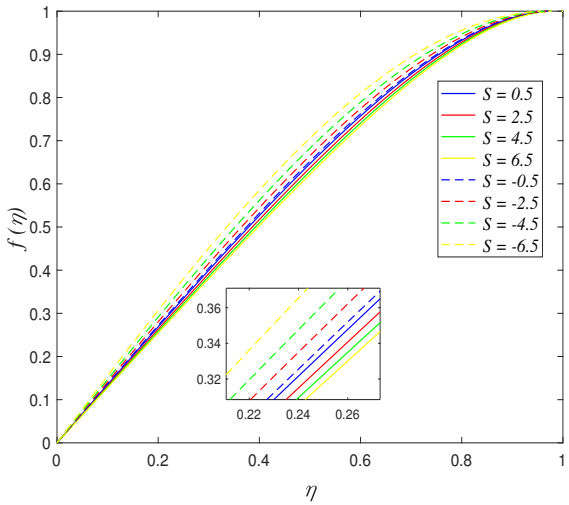

Figure 2. Impact of S on radial velocity.

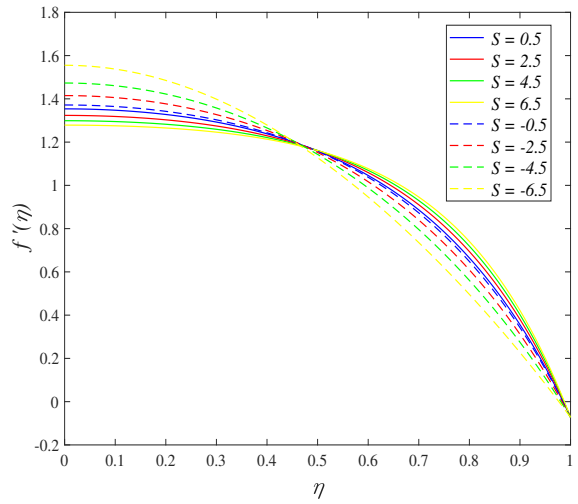

Figure 3. Impact of S on axial velocity.

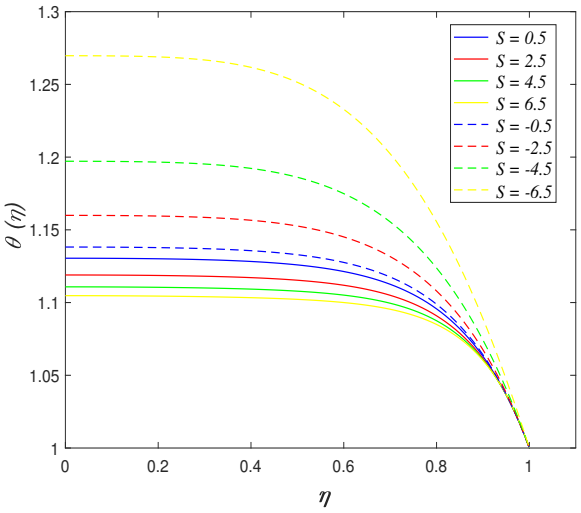

Figure 4. Impact of S on temperature.

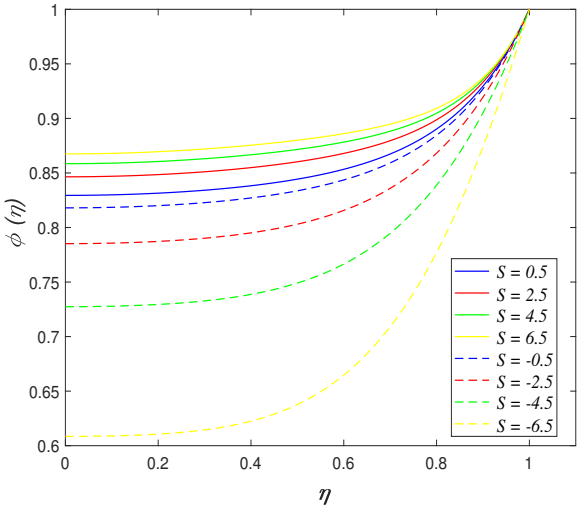

Figure 5. Impact of S on concentration.

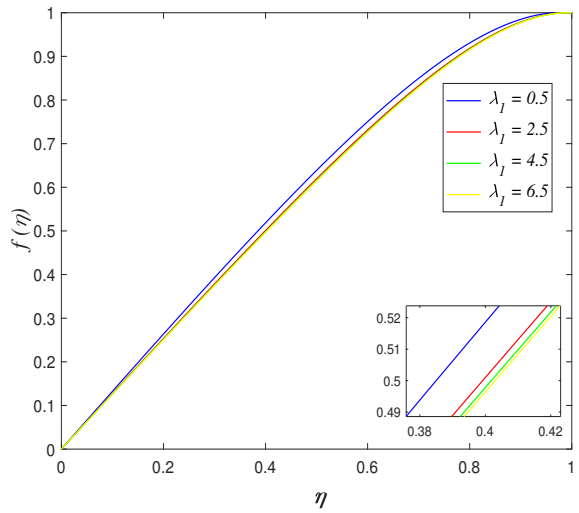

Figure 6. Impact of λ_1 on radial velocity.

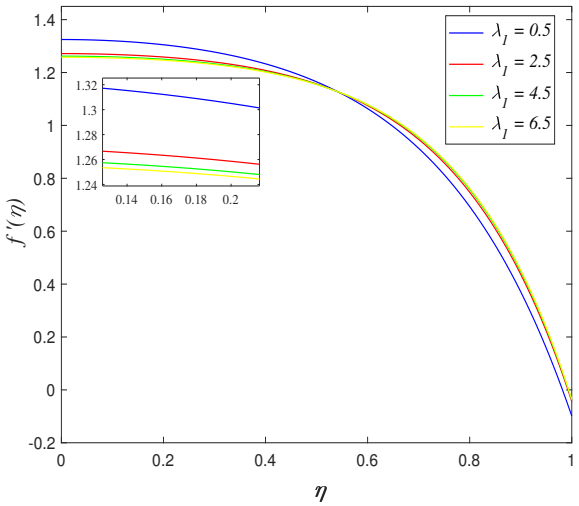

Figure 7. Impact of λ_1 on axial velocity.

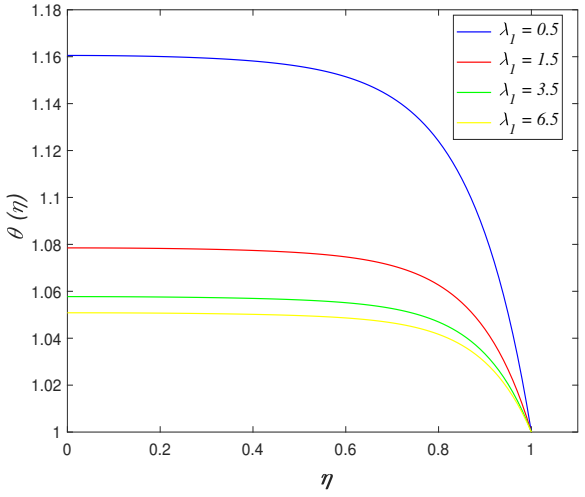

Figure 8. Impact of λ_1 on temperature.

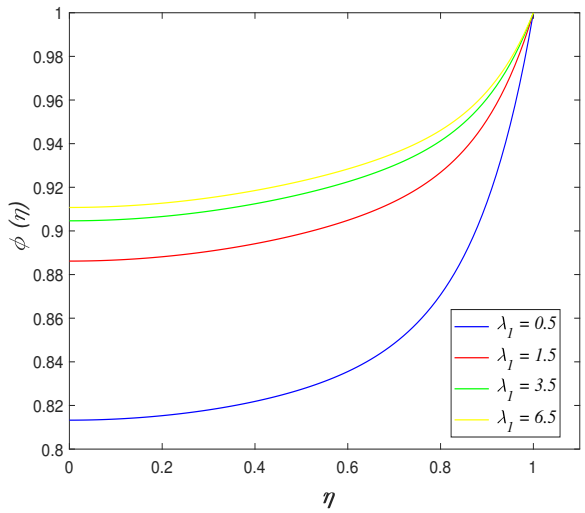

Figure 9. Impact of λ_1 on concentration.

The impacts of *Ha* on velocity, temperature and concentration are displayed in Figures 10–13. The radial velocity slows down with an increase in *Ha*. The Lorentz force is produced by the induction of a magnetic field in the flow. It raises the resistance towards the flow in the channel. The axial velocity, as shown in Figure 11, decreases for $\eta \leq 0.5$, and it accelerates for $\eta > 0.5$ when *Ha* increases. The crossflow is observed at the center of the boundary layer. The effect of *Ha* on the temperature field is presented in Figure 12. It is found that the flow temperature reduces for $\eta \leq 0.9$, and it increases for $\eta > 0.9$ for a rise of *Ha*. Figure 13 describes the variation of Ha on nanoparticle concentration. The concentration profile rises on $\eta \leq 0.85$, and it drops on $\eta > 0.85$ with a rise in Ha.

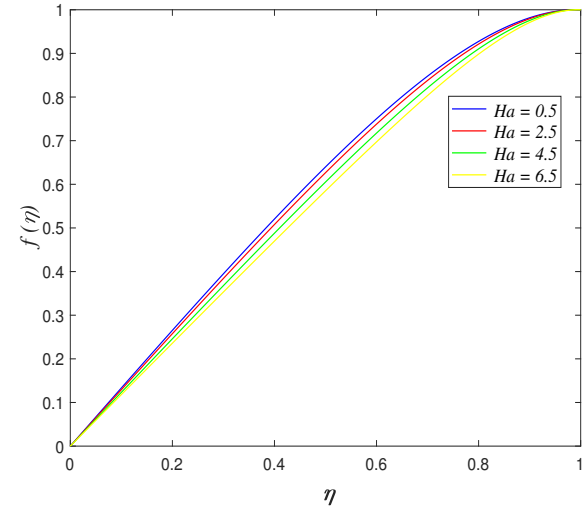

Figure 10. Impact of *Ha* on radial velocity.

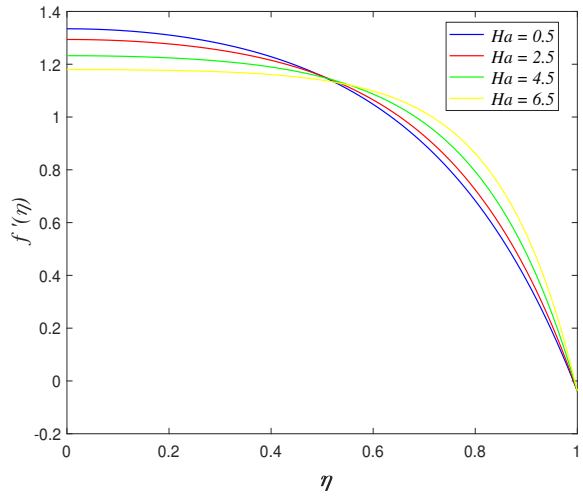

Figure 11. Impact of *Ha* on axial velocity.

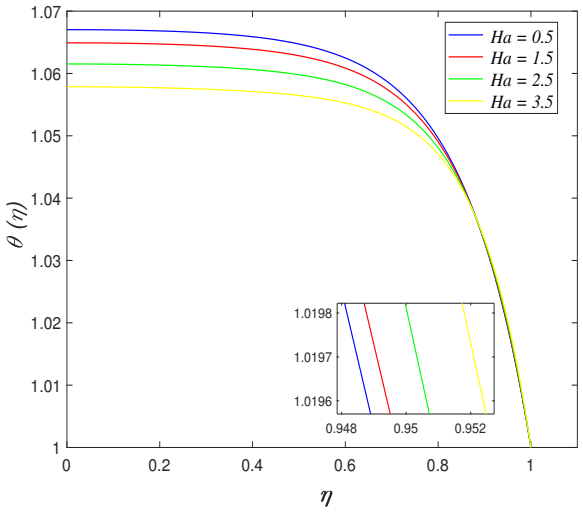

Figure 12. Impact of *Ha* on temperature.

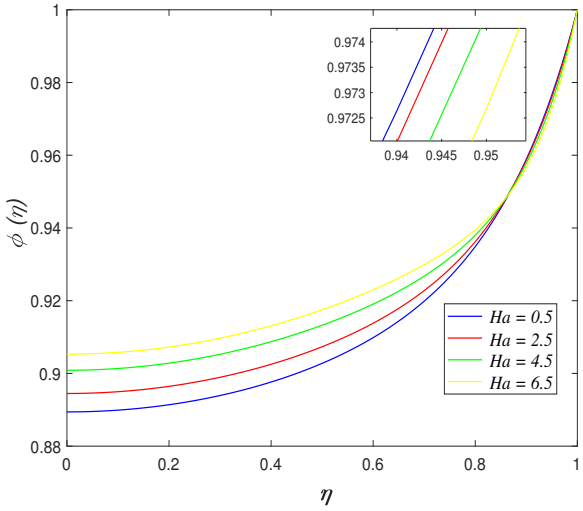

Figure 13. Impact of *Ha* on concentration.

The variation of Da on axial velocity is demonstrated in Figure 14. The velocity enhances for $\eta \leq 0.5$, and it declines for $\eta > 0.5$ when Da increases. The flow across porous medium accelerates with the rise of permeability of the porous medium. The impact of γ on axial velocity is portrayed in Figure 15. Physically, the slip condition at the upper plate is considered when the velocity at the plate and the fluid velocity nearer the plate is different. The velocity increases for $\eta \leq 0.6$, and it decreases for $\eta > 0.6$ for a rise in γ values. The reduction of flow nearer the upper wall is due to the reason that more fluid is able to slip over the wall as γ rises. The influence of De on axial velocity is presented in Figure 16. It is noticed that the velocity accelerates nearby the lower wall, and it decelerates nearby the upper wall with a rise in De. The ratio of retardation time and observation time is defined as the Deborah number. The slow reaction to an applied stress or 'delay of elasticity' is called retardation time. It is found that the rise in De implies that the fluid exhibits a longer retardation time, which causes the viscosity of the fluid to increase. Hence, the intermolecular forces of fluid particles strengthen, which leads to the flow close to the upper wall slowing down.

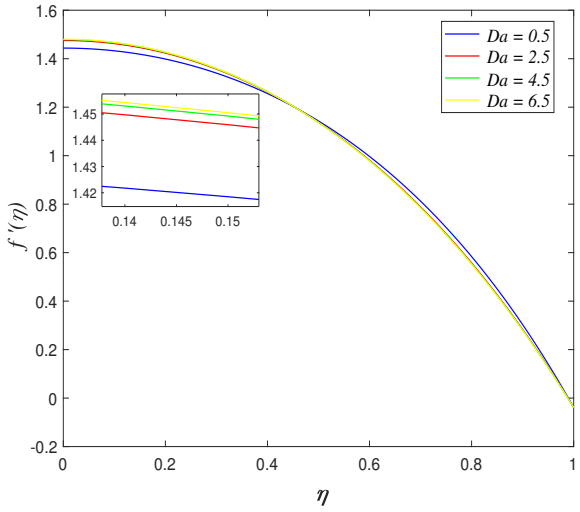

Figure 14. Impact of Da on axial velocity.

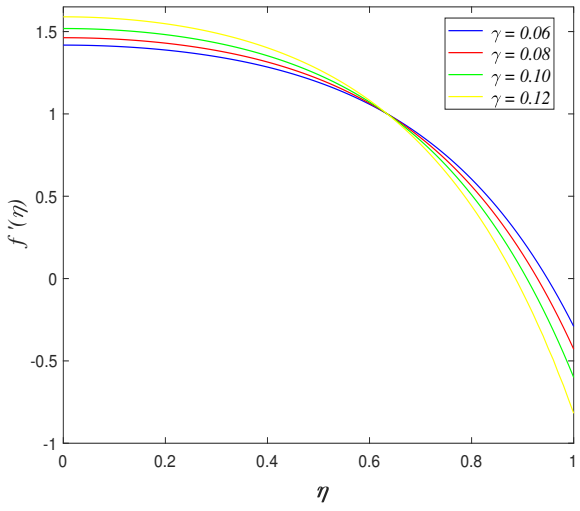

Figure 15. Impact of γ on axial velocity.

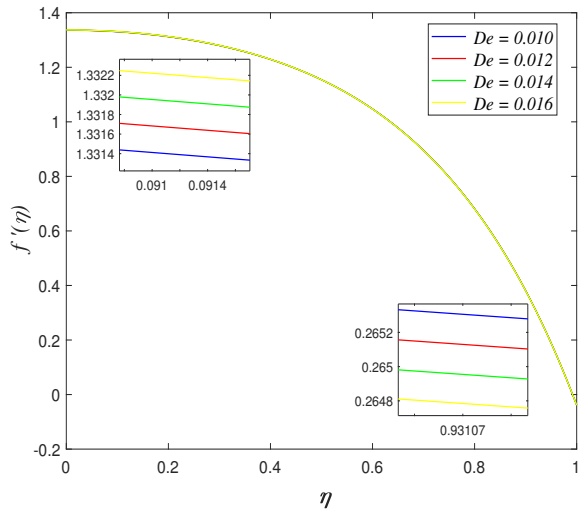

Figure 16. Impact of *De* on axial velocity.

The influence of *Pr* on the temperature field is demonstrated in Figure 17. The flow temperature elevates with a rise in *Pr*. The Prandtl number is the ratio of momentum diffusivity and thermal diffusivity. It is discovered that the enhancement of *Pr* promotes the specific heat capacity of the fluid. It has improved the fluid capability to absorb heat, which results in elevation of the flow temperature. Figure 18 portrays the effect of *Ec* on the temperature field. It is shown that the flow temperature elevates as *Ec* rises. The presence of viscous dissipation is denoted by the Eckert parameter. High values of *Ec* accelerate the kinetic energy in the fluid particles. It is converted to heat energy and thus, causes a rise in the temperature profile at the flow boundary. The impact of N_b on the temperature field is described in Figure 19. It is found that the temperature decreases when N_b rises. The movement of nanoparticles suspended in the fluid is known as Brownian motion. It is a key factor that promotes the thermal conductivity of nanofluid. The temperature in the flow decreases because of the high efficiency of heat transfer. Figure 20 discovers the variation of N_t on the temperature field. The flow temperature is enhanced with increments of N_t. The thermophoretic force is imposed on nanoparticles when there is a temperature difference within the flow and the upper boundary. The kinetic energy of nanoparticles increases due to the thermophoretic force. This phenomenon elevates the temperature profile.

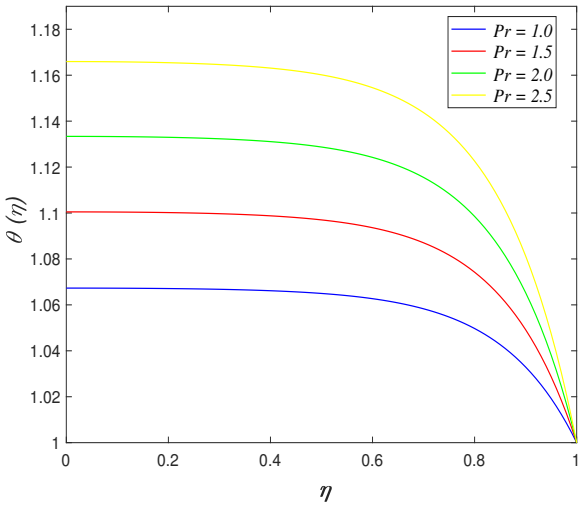

Figure 17. Impact of *Pr* on temperature.

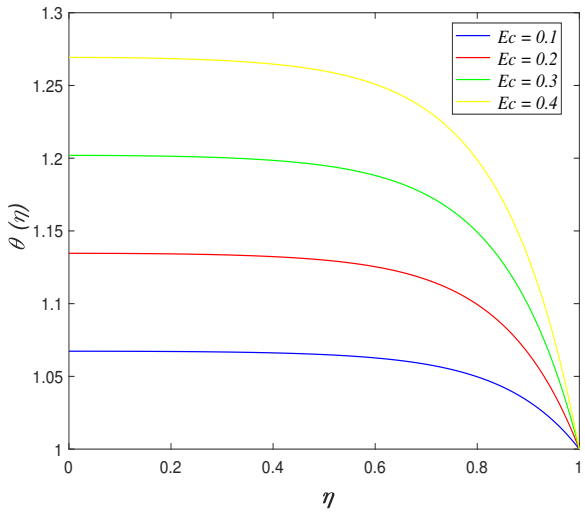

Figure 18. Impact of Ec on temperature.

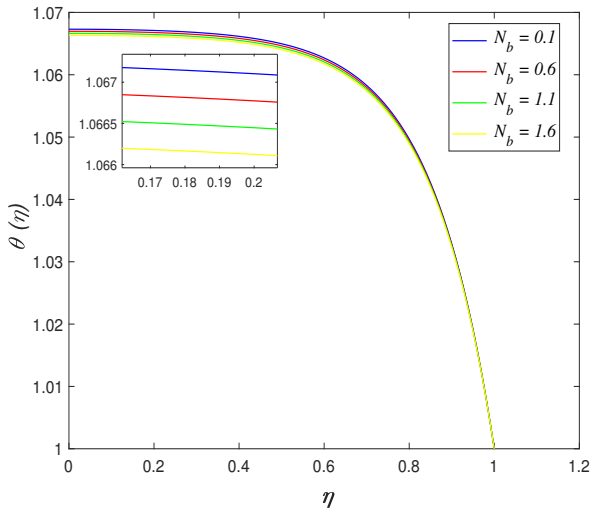

Figure 19. Impact of N_b on temperature.

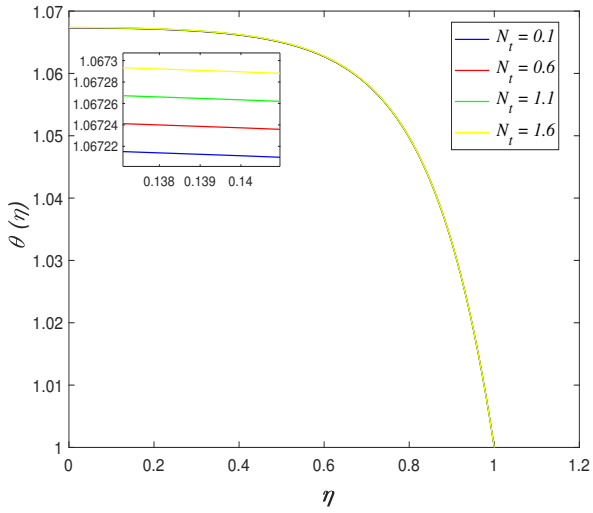

Figure 20. Impact of N_t on temperature.

Figure 21 presents the variation of N_b on nanoparticle concentration. The concentration profile rises when N_b increases. Physically, the existence of Brownian motion enhances the kinetic energy of nanoparticles. The nanoparticles move from the upper wall to the flow region effectively and, thus, increase the concentration field. The influence of N_t on nanoparticle concentration is exhibited in Figure 22. It is noted that fluid concentration decreases when N_t rises. The movement of nanoparticles from the flow region to the upper wall increases due to the thermophoretic force, which causes a reduction of the concentration profile. Figure 23 describes the variation of Le on nanoparticle concentration. The nanoparticle concentration drops with an increase in Le. It is stated that the Lewis number is inversely proportional to the Brownian motion. The motion of nanoparticles from the upper boundary to the flow region slows down as the Brownian motion decelerates. This phenomenon reduces the concentration in the fluid flow. The impacts of R on the concentration field are demonstrated in Figure 24. The influences of a chemical reaction are categorized as destructive and constructive. It is shown that nanoparticle concentration elevates in a constructive chemical reaction $(R < 0)$, and it declines in a destructive chemical reaction $(R > 0)$. The constructive chemical reaction increases the rate of reaction in the flow and, consequently, increases the fluid concentration.

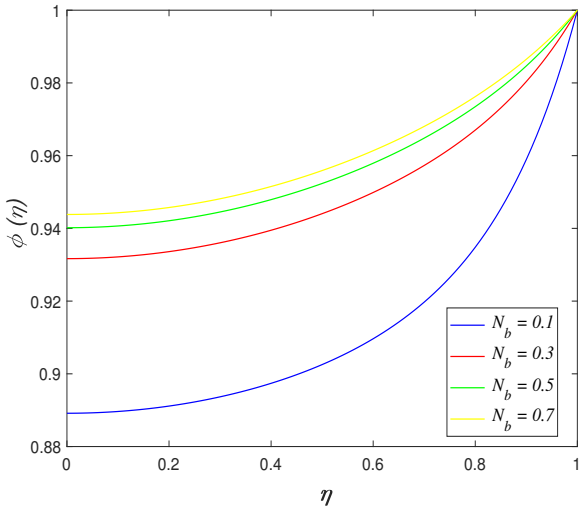

Figure 21. Impact of N_b on concentration.

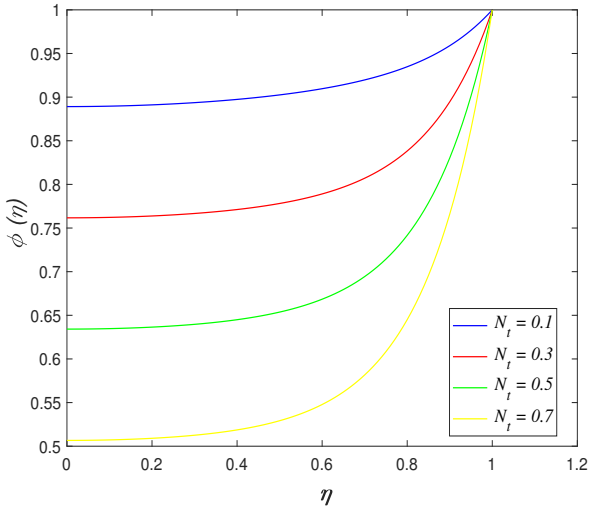

Figure 22. Impact of N_t on concentration.

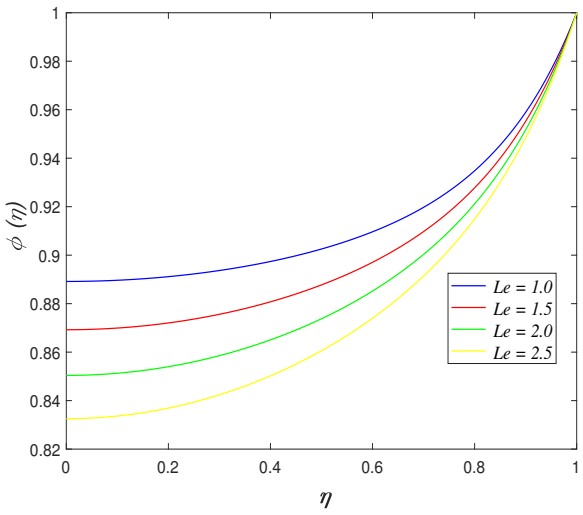

Figure 23. Impact of *Le* on concentration.

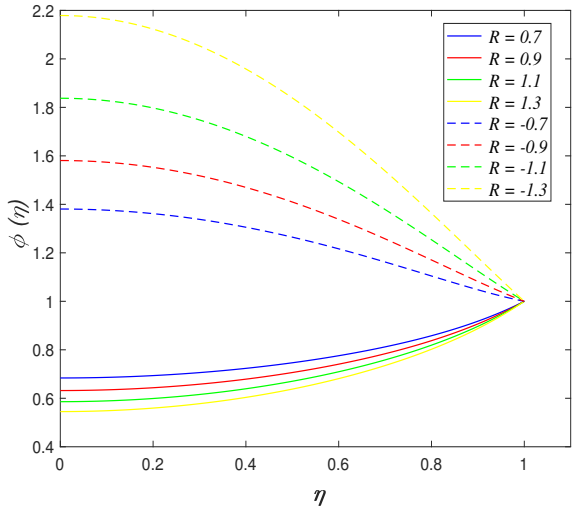

Figure 24. Impact of *R* on concentration.

4. Physical Quantities of Interest

Skin friction coefficient, Nusselt and Sherwood numbers are the physical quantities in the flow. The friction of the fluid near the wall against the wall boundary is known as the skin friction parameter. Moreover, Nusselt and Sherwood parameters are the non-dimensional parameters that describe the rate of heat and mass transfer of fluid adjacent to the wall. The definitions of the skin friction coefficient Cf_x, Nusselt number Nu_x and Sherwood number Sh_x are denoted by [51]

$$Cf_x = \frac{\tau_w}{\rho_f v_w^2}, Nu_x = \frac{lq_w}{\alpha_f T_w}, Sh_x = \frac{lq_s}{D_B C_w}, \tag{14}$$

where τ_w, q_w and q_s are the skin friction, heat and mass flux on the plate. The expressions of τ_w, q_w and q_s are given as

$$\tau_w = \mu_B\left(1 + \frac{1}{\lambda_1}\right)\left[\frac{\partial u}{\partial y}\right]_{y=h(t)}, q_w = -\alpha_f\left[\frac{\partial T}{\partial y}\right]_{y=h(t)}, q_s = -D_B\left[\frac{\partial C}{\partial y}\right]_{y=h(t)}. \tag{15}$$

The non-dimensional forms of Cf_x, Nu_x and Sh_x are

$$\begin{aligned} \frac{l^2}{x^2}(1-\alpha t)Re_x Cf_x &= \left(1+\frac{1}{\lambda_1}\right)f''(1), \\ \sqrt{(1-\alpha t)}Nu_x &= -\theta'(1), \\ \sqrt{(1-\alpha t)}Sh_x &= -\phi'(1). \end{aligned} \tag{16}$$

Numerical results of the physical quantities when varying the dimensionless parameters are illustrated in Tables 4–7. The impact of S on the skin friction coefficient, Nusselt and Sherwood numbers is presented in Table 4. The wall shear stress elevates as S rises, whereas the reverse impact is noted in the rate of heat and mass transfer. It is found that the frictional force on the fluid and the wall boundary enhances because the fluid accelerates as the plates move closer. In contrast, the reduction of the mass and heat transfer rate is owed to the kinetic energy of nanoparticles decreases in the narrow channel. Table 5 reveals the effect of S, λ_1, De, Ha, Da and γ on the skin friction coefficient. The wall shear stress rises with an increase in S, Ha and γ, whereas it slows down for increasing λ_1, Da and De. The Lorentz force and slip condition increases the friction force near the wall surface. Meanwhile, the rise in λ_1 and De enhances the viscosity of Jeffrey fluid, which results in a decline in the velocity profile. The flow nearby the upper wall also decelerates as Da increases. Therefore, the decline in the fluid velocity causes the wall shear stress to decrease. The variation of Ec, Pr, N_b and N_t on the Nusselt number is portrayed in Table 6. The Nusselt number is the ratio of thermal transfer by convection and thermal transfer by diffusion. It is noticed that Ec, Pr and N_t raise the heat transfer rate, while N_b reduces the heat transfer rate. Based on Figures 17, 18 and 20, the flow temperature elevates with increasing Ec, Pr and N_t. It has caused the kinetic energy of nanoparticles to become stronger and, therefore, enhance the rate of the heat transfer. In contrast, Brownian motion reduces the temperature profile, as exhibited in Figure 19. The deceleration of kinetic energy of nanoparticles causes the rate of the heat transfer to decrease. Table 7 demonstrates the impact of Le, R, N_b and N_t on the Sherwood number. It is discovered that the rate of mass transfer elevates with an enhancement of Le, R and N_t, whereas it drops when N_b rises. The Sherwood number is the ratio of convective mass transfer and the diffusive mass transfer. Physically, the increment of Brownian motion enhances the diffusive mass transfer, which causes the nanoparticle concentration in the flow to elevate, as displayed in Figure 21. The Sherwood number is inversely proportional to the diffusive mass transfer. Hence, this phenomenon causes a decrease in the Sherwood number. The reverse behavior is found for increments of Le, R and N_t. A high Sherwood number implies that the presence of Le, R and N_t increases the mass transfer due to convection.

Table 4. Numerical results of $-(1+1/\lambda_1)f''(1)$, $-\theta'(1)$ and $\phi'(1)$ for S when $De = \gamma = 0.01$, $\delta = Ha = Ec = N_b = N_t = 0.1$, $\lambda_1 = Da = 1$ and $Pr = Le = R = 1.5$.

S	$-(1+1/\lambda_1)f''(1)$	$-\theta'(1)$	$\phi'(1)$
−2.5	4.727939	1.244305	2.526508
−2.0	5.210547	1.158067	2.403976
−1.5	5.653556	1.097885	2.308981
−1.0	6.063763	1.055755	2.233626
−0.5	6.446384	1.026437	2.172665
0	6.805498	1.006412	2.122519
0.5	7.144352	0.993229	2.080659
1.0	7.465567	0.985166	2.045278
1.5	7.771288	0.980981	2.015046
2.0	8.063291	0.979766	1.988971
2.5	8.343065	0.980837	1.966294

Table 5. Numerical outputs of $-(1+1/\lambda_1)f''(1)$ for S, λ_1, Ha, Da, De and γ when $\delta = Ec = N_b = N_t = 0.1$ and $Pr = Le = R = 1.5$.

S	λ_1	Ha	Da	γ	De	$-(1+1/\lambda_1)f''(1)$
−1.5	1.5	0.1	1	0.01	0.01	4.444929
−1.0						4.866867
−0.5						5.253721
0						5.611752
0.5						5.945698
1.0						6.259225
1.5						6.555223
1.0	1.0	0.1	1	0.01	0.01	7.465567
	1.5					6.259225
	2.0					5.664561
	2.5					5.310315
	3.0					5.075164
	3.5					4.907676
1.0	1.5	1.0	1.0	0.01	0.01	6.430432
		1.5				6.640604
		2.0				6.924462
		2.5				7.273334
		3.0				7.678004
		3.5				8.129483
1.0	1.5	0.1	1.0	0.01	0.01	6.259225
			1.5			6.161199
			2.0			6.111640
			2.5			6.081726
			3.0			6.061708
			3.5			6.047372
1.0	1.5	0.1	1.0	0.01	0.01	6.259225
				0.03		6.985274
				0.05		7.901794
				0.07		9.093433
				0.09		12.208567
1.0	1.5	0.1	1.0	0.01	0.010	6.259225
					0.011	6.258774
					0.012	6.258324
					0.013	6.257884
					0.014	6.257454

Table 6. Numerical outputs of $-\theta'(1)$ for Ec, Pr, N_b and N_t when $De = \gamma = 0.01$, $Ha = \delta = 0.1$, $S = Da = 1$ and $\lambda_1 = Le = R = 1.5$.

Ec	Pr	N_b	N_t	$-\theta'(1)$
0.1	1.5	0.1	0.1	0.806612
0.2				1.620920
0.3				2.443096
0.4				3.273315
0.5				4.111761
0.6				4.958621
0.1	1.0	0.1	0.1	0.547527

Table 6. *Cont.*

Ec	Pr	N_b	N_t	$-\theta'(1)$
	1.5			0.806612
	2.0			1.057583
	2.5			1.301498
	3.0			1.539288
0.1	1.5	0.2	0.1	0.783219
		0.4		0.739423
		0.6		0.699276
		0.8		0.662416
		1.0		0.628517
0.1	1.5	0.1	0.2	0.810460
			0.4	0.818329
			0.6	0.826437
			0.8	0.834797
			1.0	0.843423

Table 7. Numerical outputs of $\phi'(1)$ for Le, R, N_b and N_t when $De = \gamma = 0.01$, $Ha = \delta = Ec = 0.1$, $S = Da = 1$ and $\gamma_1 = Pr = 1.5$.

Le	R	N_b	N_t	$\phi'(1)$
0.5	1.5	0.1	0.1	1.319558
1.0				1.655833
1.5				1.912033
2.0				2.121145
2.5				2.299830
3.0				2.457446
1.5	−1.5	0.1	0.1	−7.357027
	−1.0			−1.463706
	−0.5			0.049833
	0.5			1.280691
	1.0			1.632325
	1.5			1.912033
1.5	1.5	0.2	0.1	1.589931
		0.4		1.429529
		0.6		1.376588
		0.8		1.350472
		1.0		1.335057
1.5	1.5	0.1	0.2	2.543099
			0.4	3.824886
			0.6	5.133900
			0.8	6.471441
			1.0	7.838907

5. Conclusions

The present numerical research examines the influences of viscous dissipation and chemical reaction on an unsteady MHD slip flow of a Jeffrey nanofluid through permeable medium. The flow occurs due to squeeze between two parallel plates. Conversion of partial differential equations to ordinary differential equations is conducted by the implementation of dimensionless variables. The numerical results are derived by the Keller-box approach, and graphical results are attained using MATLAB. A comparison of the present results with existing reported works is conducted and shown in excellent agreement. The effects of S, λ_1, Ha, Da, γ, De, Pr, Ec, N_b, N_t, Le and R on velocity, temperature and nanoparticle concentration are analyzed. The significant findings in the investigation are summarized as:

1. The flow velocity increases as the plates move closer $(S > 0)$ and it decreases as the plates move apart $(S < 0)$ near the vicinity of the upper plate.

2. The wall shear stress increases as S, γ and Ha rise, while it reduces with an increase in λ_1, Da and De.
3. The enhancement of λ_1 and Ha decelerate the fluid velocity, temperature, and concentration.
4. The flow velocity adjacent to the upper plate region slows down for increasing γ, Da and De.
5. The fluid temperature and heat transfer rate enhance when Pr, Ec and N_t increases, whereas the opposite effect is observed with an increase in N_b.
6. The rise of N_b increases the nanoparticle concentration and decreases the mass transfer rate.

Author Contributions: Conceptualization, N.A.M.N. and M.A.A.; methodology, N.A.M.N.; software, N.A.M.N.; validation, N.A.M.N., M.A.A. and S.S.; writing—original draft, N.A.M.N.; writing—review and editing, N.A.M.N.; supervision, M.A.A. and S.S. All authors have read and agreed to the published version of the manuscript.

Funding: This research was funded by the Ministry of Education (MOE) and Research Management Centre of Universiti Teknologi Malaysia (UTM), FRGS/1/2019/STG06/UTM/02/22, 5F004, 5F278, 07G70, 07G72, 07G76, 07G77 and 08G33.

Conflicts of Interest: The authors declare no conflict of interest.

Abbreviations

The following abbreviations are used in this manuscript:

Roman letters

B	magnetic field
c_f	concentration susceptibility
c_p	specific heat of nanoparticles
C	nanoparticle concentration
C_w	concentration at upper plate
D_B	Brownian diffusion coefficient
D_T	Thermophoretic diffusion coefficient
De	Deborah Number
Da	Darcy Number
Ec	Eckert Number
Ha	Hartmann number
h	distance between two plates
k_1	permeability of porous medium
k_f	thermal conductivity of fluid
k_c	rate of chemical reaction
Le	Lewis number
l	initial distance between two surfaces (at $t = 0$)
N_1	velocity slip
N_b	Brownian motion parameter
N_t	thermophoresis parameter
Pr	Prandtl number
S	squeeze number
R	chemical reaction parameter
T	fluid temperature
T_w	temperature at upper plate
T_m	ambient temperature
t	time
u	fluid velocity in x direction
v	fluid velocity in y direction
v_w	velocity at upper plate

(x, y) cartesian coordinates

Greek symbols

α constant
α_f thermal diffusivity of Jeffrey fluid
γ slip parameter
f dimensionless velocity parameter
θ dimensionless temperature parameter
δ dimensionless length
ϕ Dimensionless concentration parameter
η boundary layer thickness
ν_f kinematic viscosity
σ electrical conductivity
ρ_f fluid density
ρ_p density of nanoparticles
φ porosity of porous medium
λ_1 ratio of relaxation to retardation times
λ_2 retardation time
τ ratio of heat capacities of nanoparticles and fluid

References

1. Eastman, J.A.; Choi, S.U.S.; Li, S.; Yu, W.; Thompson, L.J. Anomalously increased effective thermal conductivities of eth-ylene glycol-based nanofluids containing copper nanoparticles. *Appl. Phys. Lett.* **2001**, *78*, 718–720. [CrossRef]
2. Wong, K.V.; De Leon, O. Applications of nanofluids: Current and future. *Adv. Mech. Eng.* **2010**. [CrossRef]
3. Buongiorno, J. Convective Transport in Nanofluids. *ASME J. Heat Transf.* **2006**, *128*, 240–250. [CrossRef]
4. Kuznetsov, A.V.; Nield, D.A. The onset of double-diffusive nanofluid convection in a layer of a saturated porous medium. *Transp. Porous Medium* **2010**, *85*, 941–951. [CrossRef]
5. Sheikholeslami, M.; Hatami, M.; Domairry, G. Numerical simulation of two phase unsteady nanofluid flow and heat transfer between parallel plates in presence of time dependent magnetic field. *J. Taiwan Inst. Chem. Eng.* **2015**, *46*, 43–50. [CrossRef]
6. Noor, N.A.M.; Shafie, S.; Admon, M.A. Effects of Viscous Dissipation and Chemical Reaction on MHD Squeezing Flow of Casson Nanofluid between Parallel Plates in a Porous Medium with Slip Boundary Condition. *Eur. Phys. J. Plus* **2020**, *135*. [CrossRef]
7. Stefan, M. Experiments on apparent adhesion. *Lond. Edinb. Dublin Philos. Mag. J. Sci.* **1874**, *47*, 465–466. [CrossRef]
8. Reynolds, O. On the theory of lubrication and its application to Mr. Beauchamp tower's experiments, including an experimental determination of the viscosity of olive oil. *Philos. Trans. R. Soc. Lond.* **1886**, *177*, 157–234. [CrossRef]
9. Archibald, F.R. Load capacity and time relations for squeeze films. *Trans. ASME* **1956**, *78*, 231–245. [CrossRef]
10. Jackson, J.D. A study of squeezing flow. Applied Scientific Research. *Trans. ASME* **1963**, *11*, 148–152. [CrossRef]
11. Ishizawa, S. The unsteady flow between two parallel discs with arbitrary varying gap width. *Bull. Jpn. Soc. Mech. Eng.* **1966**, *9*, 533–550. [CrossRef]
12. Leider, P.J.; Bird, R.B. Squeezing Flow between Parallel Disks: Theoretical Analysis. *Ind. Eng. Chem. Fundam.* **1974**, *13*, 336–341. [CrossRef]
13. Grimm, R.J. Squeezing flows of Newtonian liquid films: An analysis including fluid inertia. *Appl. Sci. Res.* **1976**, *32*, 149–166. [CrossRef]
14. Wang, C.Y. The squeezing of a fluid between two plates. *J. Appl. Mech.* **1976**, *43*, 579–583. [CrossRef]
15. Bujurke, N.M.; Achar, P.K.; Pai, N.P. Computer extended series for squeezing flow between plates. *Fluid Dyn. Res.* **1995**, *16*, 173–187. [CrossRef]
16. Noor, N.A.M.; Shafie, S.; Admon, M.A. Unsteady MHD squeezing flow of Jeffrey fluid in a porous medium with thermal radiation, heat generation/absorption and chemical reaction. *Phys. Scr.* **2020**, *95*. [CrossRef]
17. Khan, U.; Ahmed, N.; Khan, S.I.; Zaidi, Z.A.; Xiao-Jun, Y.; Mohyud-Din, S.T. On unsteady two-dimensional and axisymmet-ric squeezing flow between parallel plates. *Alex. Eng. J.* **2014**, *53*, 463–468. [CrossRef]
18. Gaffar, S.A.; Prasad, V.R.; Bég, O.A. Numerical study of flow and heat transfer of non-Newtonian tangent hyperbolic fluid from a sphere with Biot number effects. *Alex. Eng. J.* **2015**, *54*, 829–841. [CrossRef]
19. Ali, A.; Asghar, S. Analytic solution for oscillatory flow in a channel for Jeffrey fluid. *J. Aerosp. Eng.* **2012**, *27*, 644–651. [CrossRef]
20. Sharma, B.D.; Yadav, P.K.; Filippov, A. A Jeffrey-fluid model of blood flow in tubes with stenosis. *Colloid J.* **2017**, *79*, 849–856. [CrossRef]
21. Mukhopadhyay, S. MHD boundary layer flow and heat transfer over an exponentially stretching sheet embedded in a thermally stratified medium. *Alex. Eng. J.* **2013**, *52*, 259–265. [CrossRef]
22. Hayat, T.; Sajjad, R.; Asghar, S. Series solution for MHD channel flow of a Jeffrey fluid. *Commun. Nonlinear Sci. Numer. Simul.* **2010**, *15*, 2400–2406. [CrossRef]

23. Muhammad, T.; Hayat, T.; Alsaedi, A.; Qayyum, A. Hydromagnetic unsteady squeezing flow of Jeffrey fluid between two parallel plates. *Chin. J. Phys.* **2017**, *55*, 1511–1522. [CrossRef]
24. Ahmad, K.; Ishak, A. Magnetohydrodynamic flow and heat transfer of a Jeffrey fluid towards a stretching vertical surface. *Therm. Sci.* **2015**. [CrossRef]
25. Hayat, T.; Abbas, T.; Ayub, M.; Muhammad, T.; Alsaedi, A. On Squeezed Flow of Jeffrey Nanofluid between Two Parallel Disks. *Appl. Sci.* **2016**, *6*, 346. [CrossRef]
26. Sheikholeslami, M.; Ganji, D.D.; Ashorynejad, H.R. Investigation of squeezing unsteady nanofluid flow using ADM. *Powder Technol.* **2013**, *239*, 259–265. [CrossRef]
27. Pourmehran, O.; Rahimi-Gorji, M.; Gorji-Bandpy, M.; Ganji, D.D. Analytical investigation of squeezing unsteady nanofluid flow between parallel plates by LSM and CM. *Alex. Eng. J.* **2014**, *54*, 17–26. [CrossRef]
28. Gorgani, H.H.; Maghsoudi, P.; Sadeghi, S. An innovative approach for study of thermal behavior of an unsteady nanofluid squeezing flow between two parallel plates utilizing artificial neural network. *Eur. J. Sustain. Dev. Res.* **2019**, *3*. [CrossRef]
29. Acharya, N.; Das, K.; Kundu, P.K. The squeezing flow of Cu-water and Cu-kerosene nanofluids between two parallel plates. *Alex. Eng. J.* **2016**, *55*, 1177–1186. [CrossRef]
30. Azimi, M.; Riazi, R. MHD unsteady GO-water squeezing nanofluid flow heat and mass transfer between two infinite parallel moving plates: Analytical investigation. *Sadhana* **2017**, *42*, 335–341. [CrossRef]
31. Sheikholeslami, M.; Ganji, D.D.; Rashidi, M.M. Magnetic field effect on unsteady nanofluid flow and heat transfer using Buongiorno model. *J. Magn. Magn. Mater.* **2016**, *416*, 164–173. [CrossRef]
32. Madaki, A.G.; Roslan, R.; Rusiman, M.S.; Raju, C.S.K. An innovative approach for study of thermal behavior of an unsteady nanofluid squeezing flow between two parallel plates utilizing artificial neural network. *Alex. Eng. J.* **2017**, *57*, 1033–1040. [CrossRef]
33. Ullah, I.; Shafie, S.; Khan, I. Soret and Dufour effects on unsteady mixed convection slip flow of Casson fluid over a nonlinearly stretching sheet with convective boundary condition. *Sci. Rep.* **2017**, *7*. [CrossRef] [PubMed]
34. Khan, U.; Ahmed, N.; Asadullah, M.; Mohyud-din, S.T. Effects of viscous dissipation and slip velocity on two dimensional and axisymmetric squeezing flow of Cu-water and Cu-kerosene nanofluids. *Propuls. Power Res.* **2015**, *4*, 40–49. [CrossRef]
35. Singh, K.; Rawat, S.K.; Kumar, M. Heat and mass transfer on squeezing unsteady MHD nanofluid flow between parallel plates with slip velocity effect. *J. Nanosci.* **2016**. [CrossRef]
36. Sobamowo, G.M.; Jayesimi, L.O. Squeezing Flow Analysis of Nanofluid Under the Effects of Magnetic Field and Slip Boundary Conditions Using Chebychev Spectral Collocation Method. *Fluid Mech.* **2017**, *3*, 54–60. [CrossRef]
37. Sobamowo, M.G.; Akinshilo, A.T.; Yinusa, A.A. Thermo-Magneto-Solutal Squeezing Flow of Nanofluid between Two Parallel 564 Disks Embedded in a Porous Medium: Effects of Nanoparticle Geometry, Slip and Temperature Jump Conditions. *Model. Simul. Eng.* **2018**. [CrossRef]
38. Ullah, I.; Bhattacharyya, K.; Shafie, S.; Khan, I. Unsteady MHD mixed convection slip flow of Casson fluid over nonlinearly stretching sheet embedded in a porous medium with chemical reaction, thermal radiation, heat generation/absorption and convective boundary conditions. *PLoS ONE* **2016**, e0165348. [CrossRef]
39. Ullah, I.; Waqas, M.; Hayat, T.; Alsaedi, A.; Khan, M. Thermally radiated squeezed flow of magneto-nanofluid between two parallel disks with chemical reaction. *J. Therm. Anal. Calorim.* **2019**, *135*, 1021–1030. [CrossRef]
40. Mohamed, R.A.; Rida, S.Z.; Arafa, A.A.M.; Mubarak, M.S. Heat and mass transfer in an unsteady Magnetohydrodynamics Al2O3-water nanofluid squeezed between two parallel radiating plates embedded in porous media with chemical reaction. *J. Heat Transf. Trans. ASME* **2020**, *142*. [CrossRef]
41. Raju, C.S.K.; Babu, M.J.; Sandeep, N. Chemically reacting radiative MHD Jeffrey nanofluid flow over a cone in porous medium. *Int. J. Eng. Res. Afr.* **2016**, *19*, 75–90. [CrossRef]
42. Shankar, U.; Naduvinamani, N.B. Magnetized impacts of Brownian motion and thermophoresis on unsteady squeezing flow 578 of nanofluid between two parallel plates with chemical reaction and Joule heating. *Heat Transf. Asian Res.* **2019**, *48*, 4174–4202. [CrossRef]
43. Noor, N.A.M.; Shafie, S.; Admon, M.A. MHD Squeezing Flow of Casson Nanofluid with Chemical Reaction, Thermal Radiation and Heat Generation/Absorption. *J. Adv. Res. Fluid Mech. Therm. Sci.* **2020**, *68*, 94–111. [CrossRef]
44. Song, J.; An, W.; Wu, Y.; Tian, W. Neutronics and Thermal Hydraulics Analysis of a Conceptual Ultra-High Temperature MHD Cermet Fuel Core for Nuclear Electric Propulsion. *Front. Energy Res.* **2018**, *6*. [CrossRef]
45. Sharma, D.; Pandey, K.M.; Debbarma, A.; Choubey, G. Numerical Investigation of heat transfer enhancement of SiO2-water based nanofluids in light water nuclear reactor. *Mater. Today Proc.* **2017**, *4*, 10118–10122. [CrossRef]
46. Noor, N.A.M.; Shafie, S.; Admon, M.A. Unsteady MHD flow of Casson nanofluid with chemical reaction, thermal radiation 592 and heat generation/absorption. *MATEMATIKA* **2019**, *35*, 33–52. [CrossRef]
47. Naduvinamani, N.B.; Shankar, U. Thermal-diffusion and thermo-diffusion effects on squeezing flow of unsteady magnetohydrodynamic Casson fluid between two parallel plates with thermal radiation. *Sadhana* **2019**, *44*. [CrossRef]
48. Mustafa, M.; Hayat, T.; Obaidat, S. On heat and mass transfer in the unsteady squeezing flow between parallel plates. *Meccanica* **2012**, *47*, 1581–1589. [CrossRef]
49. Gupta, A.K.; Ray, S.S. Numerical treatment for investigation of squeezing unsteady nanofluid flow between two parallel plates. *Powder Technol.* **2015**, *279*, 282–289. [CrossRef]

50. Celik, I. Squeezing flow of nanofuids of Cu-water and kerosene between two parallel plates by Gegenbauer wavelet collocation method. *Eng. Comput.* **2019**. [CrossRef]
51. Noor, N.A.M.; Shafie, S.; Admon, M.A. Impacts of chemical reaction on squeeze flow of MHD Jeffrey fluid in horizontal porous channel with slip condition. *Phys. Scr.* **2021**, *96*. [CrossRef]